The Assessment of Upper-Limb Spasticity Based on a Multi-Layer Process Using a Portable Measurement System

Chen Wang, Liang Peng, Zeng-Guang Hou, *Fellow, IEEE*, and Pu Zhang

***Abstract*— Spasticity is a common disabling complication caused by the upper motor neurons dysfunction following neurological diseases such as stroke. Currently, the assessment of the spastic hypertonia triggered by stretch reflexes is manually performed by clinicians using perception-based clinical scales, however, their reliability is still questionable due to the inter-rater and intra-rater variability. In order to objectively quantify the complex spasticity phenomenon in post-stroke patients, this study proposed a multi-layer assessment system based on a novel measurement device. The exoskeletal device was developed to synchronously record the kinematic, biomechanical and electrophysiological information in sixteen spastic patients and ten age-matched healthy subjects, while the spastic limb was stretched at low, moderate and high velocities. The mechanical impedance of the elbow joint was identified using a modified genetic algorithm to quantify the alterations in viscoelastic properties underlying pathological resistance. Simultaneously, the time-frequency features were extracted from the surface electromyography (sEMG) signals to reveal the neurophysiological mechanisms of the spastic muscles. By concatenating these single-layer decisions, a support vector regression (SVR)-based fusion model was developed to generate a more comprehensive quantification of spasticity severity. Experimental results demonstrated that the stiffness and damping components of the spastic arm significantly deviated from the nonspastic baseline, and strong correlations were observed between the proposed spasticity assessment and the severity level measured by clinical scales ($R = 0.86$, $P = 1.67e-5$), as well as the tonic stretch reflex threshold (TSRT) value ($R = -0.89$, $P = 3.54e-6$). These promising results suggest that the proposed assessment system holds great potential to support the clinical diagnosis of motor abnormalities in spastic patients, and ultimately enables optimal adjustment of treatment protocols.**

***Index Terms*— Spasticity quantification, portable assessment device, modified genetic algorithm, ensemble empirical mode decomposition (EEMD), multi-layer fusion.**

Manuscript received August 3, 2021; revised September 10, 2021; accepted October 7, 2021. Date of publication October 21, 2021; date of current version November 3, 2021. This work was supported in part by the National Natural Science Foundation of China under Grant U1913601 and Grant 61720106012, in part by the Major Scientific and Technological Innovation Projects in Shandong Province under Grant 2019JZZY011111, and in part by the Strategic Priority Research Program of Chinese Academy of Sciences under Grant XDB32040000. *(Corresponding author: Zeng-Guang Hou.)*

This work involved human subjects or animals in its research. Approval of all ethical and experimental procedures and protocols was granted by the Ethics Committee of China Rehabilitation Research Center.

Chen Wang and Liang Peng are with the State Key Laboratory of Management and Control for Complex Systems, Institute of Automation, Chinese Academy of Sciences, Beijing 100190, China (e-mail: wangchen2016@ia.ac.cn; liang.peng@ia.ac.cn).

Zeng-Guang Hou is with the State Key Laboratory of Management and Control for Complex Systems, Institute of Automation, Chinese Academy of Sciences, Beijing 100190, China, also with the School of Artificial Intelligence, University of Chinese Academy of Sciences, Beijing 100049, China, and also with the CAS Center for Excellence in Brain Science and Intelligence Technology, Beijing 100190, China (e-mail: zengguang.hou@ia.ac.cn).

Pu Zhang is with China Rehabilitation Research Center, Beijing Bo'ai Hospital, Beijing 100068, China (e-mail: jump.zp@163.com).

Digital Object Identifier 10.1109/TNSRE.2021.3121780

I. Introduction

SPASTICITY is a motor disorder induced by the hyperexcitability of tonic stretch reflexes [1], resulting in a velocity-dependent increase in muscle tone with exaggerated tendon jerk, as a common clinical manifestation of upper motor neuron syndrome following central nervous system injuries [2]–[4]. The pathophysiology of spasticity leads to movement disorders and functional disability [5], [6], and therapeutic techniques (e.g. physical and surgical treatments) are currently available to control the disease progression [7]. In clinical settings, reliable assessment of spasticity is essential for individualizing the optimal treatment, measuring the treatment efficacy and monitoring the patients' functional recovery [8], [9].

At present, the clinical assessment of spasticity is accomplished by manually perceiving limb resistance based on rating scales (e.g. Ashworth Scale [10], Modified Ashworth Scale (MAS) [11], Tardieu Scale [12], and Modified Tardieu Scale (MTS) [13]). Among these scales for spasticity assessment, MAS is most widely accepted since it has easy-to-use procedures, for example, clinicians judge the amount of muscle resistance during the stretch of patient's relaxed muscles by using qualitative terms such as no increase (MAS 0), slight increase (MAS 1 and 1+), more marked increase (MAS 2) and considerable increase (MAS 3). However, MAS does not consider the velocity-dependent phenomenon in the induced stretch reflex, and ignores the evaluation of neural component in spasticity. Furthermore, the inter-rater and intra-rater reliability of these clinical scales has been questioned due to the intrinsic limitations of "feel the resistance" [14]–[16].

This work is licensed under a Creative Commons Attribution 4.0 License. For more information, see https://creativecommons.org/licenses/by/4.0/

TABLE I
AN OVERVIEW OF STUDIES IN THE ASSESSMENT OF UPPER EXTREMITY SPASTICITY

Reference	Patient Set	Etiology	Sensors	Annotation Method	Model	Severity Estimation	Performance
[17]	20	Stroke	Electrogoniometer and electromyography	MAS	Linear regression model	TSRT	Inter-rater and intra-rater reliability: 0.46-0.68 and 0.53-0.68
[18]	15	Stroke	Electrogoniometer and electromyography	MAS	Linear regression model and K-means clustering algorithm	K-means clustering of the TSRTs	Consistency between MAS scores and new groups: 66.7%
[19]	25	Cerebral palsy, multiple sclerosis and spinal cord injury	Fibre-optic goniometer and electromyography	Re-assigned MAS	Sensor-based metric extraction	Maximal kinematic and EMG deviations from reference at spastic onset	Metrics were correlated positively with MAS scores
[20]	21	Stroke	Angular sensor and electromyography	MAS	Hilbert-Huang transform marginal spectrum entropy based method	SRO and K-means clustering of the DSRT/PROMs	SRO recognition rate: 95.45%, correlation between MAS and the DSRT index: -0.824 - -0.900
[21]	10	Stroke	Dynamic splint	FMA and MAS	Finite element analysis	Clinical index	Effectively manage and assess the hand spasticity
[22]	15	Stroke	Wireless IMUs	MAS	Musculoskeletal upper limb modelling	TSRT	Correlation between MAS scores and the severity rankings: 0.821
[23]	39	Stroke	Accelerometer mechanomyography (ACC-MMG) and electromyography	MAS	Support vector machine (linear kernel, radial basis function and sigmoid kernel)	Time and frequency domain features of sEMG-MMG	Classification accuracies for sEMG, MMG, and sEMG-MMG: 70.9%, 83.3%, and 91.7%

Recently, growing interest in the neurophysiological and biomechanical analysis of spasticity has emerged to quantify the severity of abnormalities in spastic patients (e.g. see Table I). In some studies, the electromyography (EMG) of flexor and extensor muscles is measured during the clinical passive stretch motion to quantify the disordered muscle activation, and there is significant correlation between the degree of spasticity and features extracted from EMG signals. In others, portable measurement systems are designed to evaluate the velocity-dependent characteristics of spastic behaviors by monitoring joint angles and angular velocities, such as the estimation of the tonic stretch reflex threshold (TSRT) [24]. Despite these studies have improved the validity and reliability of spasticity assessment, there is still no comprehensive quantification method simultaneously emphasizing on kinematic, biomechanical and electrophysiological information of the induced stretch motion.

Indeed, researches in animals and humans have suggested that the velocity-dependent stretch reflex threshold (SRT) is a more promising index in the severity quantification of spasticity [25], [26], which reflects the motor control impairments in the Lance's definition of spasticity. More concretely, the TSRT identifies the joint angle at which the motor unit recruitment first appears with zero stretch velocity, and can be estimated based on the regression model of the dynamic stretch reflex threshold (DSRT) [24]. Usually, the DSRT is expressed as the joint angle and angular velocity at which the standard deviation of EMG signals increases by more than 2 times, and the biomechanical response of involuntary stretch reflexes is of little concern. In order to provide a deeper insight into impairments of neuromusculoskeletal function in spastic patients, it is crucial to explore not only the neurophysiological mechanisms, but also the inertial, viscous and elastic characteristics of the affected extremity underlying the resistance perceived by clinicians.

In this study, we introduce a multi-layer assessment system to reliably quantify the severity of spastic hypertonia in post-stroke patients. An exoskeletal assessment device was developed to synchronously measure the kinematic, biomechanical and electrophysiological responses evoked by limb stretches, and a range of stretch velocities were designed to explore the velocity-dependent characteristics of spasticity. In order to address the alterations in viscoelastic properties of the spastic arm, we employed the genetic algorithm (GA)-based approach to identify the mechanical impedance components of the human elbow joint, which plays a pivotal role in quantifying the spastic resistance perceived by the clinician. As the disordered motor control in spastic patients is strongly related to abnormal neural activation patterns, the non-stationary surface electromyography (sEMG) signals were decomposed into multi-frequency oscillations based on the empirical mode decomposition (EEMD), and a series of statistical features (e.g. co-activation ratio) were extracted for neurophysiological analysis. Furthermore, to yield a more comprehensive assessment of spasticity phenomenon, the identified mechanical impedance and the relevant electrophysiological features were fused by a multi-level regression model using the supervised machine learning algorithm. Under the proposed assessment system, the pathology severity of upper-limb spasticity was automatically quantified into an easy-to-understand index with multi-level detailed diagnosis.

Our contributions in quantitatively evaluating the severity of spasticity comprise three key methodological achievements:

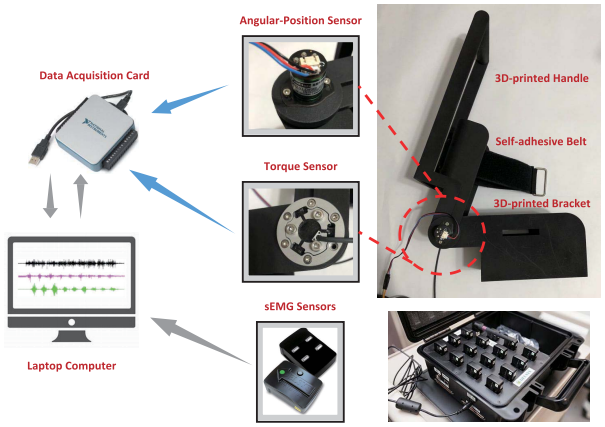

Fig. 1. Overview of the spasticity assessment system. The angular-position sensor and torque sensor are mounted on the 3D-printed structures, and the sEMG electrodes can be directly attached to the upper-limb muscles. Multi-modal data were synchronously measured during the induced stretch movements.

- An exoskeletal spasticity assessment device was designed to induce stretch reflex responses at different velocities, as well as record multi-modal information underlying the spasticity phenomenon.
- The mechanical impedance of elbow joint was identified to quantify the biomechanical abnormalities of the spastic hypertonia, and the neurophysiological feature was extracted to characterize the clinical manifestation of spastic muscles.
- A multi-layer fusion modal was constructed to generate an overall quantification of the kinematic, biomechanical and electrophysiological disorders that impair the motor function in spastic patients.

The remaining parts of this study are organized as follows: Section II introduces the spasticity assessment device and multi-modal data acquisition process, and then Section III details the experimental methodology including subject recruitment, experimental set-up and data preprocessing. Section IV presents the multi-layer architecture for spasticity assessment, and experimental results are detailed in Section V. Finally, Section VI discusses the results and concludes the paper.

II. Spasticity Assessment System

A. Mechanical Structure

We have developed a novel spasticity assessment device (see Fig. 1) to capture the kinematic, biomechanical and electrophysiological abnormalities during the induced stretch motion. The device mainly consists of 3D-printed handle and bracket, as well as a multi-modal data acquisition module. The main body can couple with the patient's upper extremity like an exoskeleton, and provide the clinician a holding handle to evoke stretch responses at different stretch velocities. Compared to the existing mechanical devices using torque motors to impose limb stretches, our assessment device focuses on quantifying the pathological phenomenon of upper-limb spasticity in clinical practices. Concretely, the data acquisition module consists of angular-position sensor (model P3022, PandAuto Inc., China), torque sensor (model M2210B5, Sunrise Instruments Inc., China) and sEMG sensors (TrignoTM Wireless System, Delsys Inc., USA), which can simultaneously measure the kinematic, biomechanical and electrophysiological responses of spastic stretch reflexes.

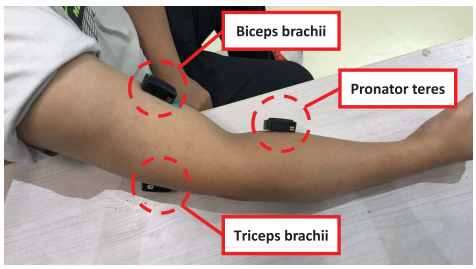

Fig. 2. The placement of surface electrodes on muscles: pronator teres, biceps brachii and triceps brachii.

B. Multi-Modal Data Acquisition

In order to quantify the elbow flexor and extensor spasticity, the rotation axis of angular-position and torque sensors were placed in line with the elbow joint axis, and sEMG sensors were fixed on forearm and upper-arm muscles (see Fig. 2). Specifically, the joint angle was acquired within the range of 0° to 180° by the angular-position sensor, and the angular velocity can be calculated accordingly. The resistance torque was recorded by the torque sensor synchronously, and then two modal signals were digitized by an A/D converter (model USB-6009, National Instruments Inc., USA) at a sampling rate of 1111.1 Hz. Simultaneously, the muscle activation was measured by sEMG electrodes and sampled at 1111.1 Hz. The acquisition of all data was transferred to a personal computer via USB port for further analysis.

III. Experimental Methodology

A. Participants and Clinical Testing

Sixteen patients with stroke-related spasticity (11 males, 5 females, mean age 51.6 ± 14.1 years) were recruited from the China Rehabilitation Research Center, and ten healthy age-matched control subjects (6 males, 4 females, mean age 48.5 ± 15.2 years) were also included in this study. The inclusion criteria for the spastic patients selection included: 1) sustained a ischemic or hemorrhagic stroke; 2) spasticity symptoms in the flexors or extensors in at least one elbow; 3) at least a 90° passive range of motion in the elbow joint (MAS score ranges from 0 to 3); 4) no anti-spasticity medication in the three months prior to the study; 5) no severe visual or cognitive impairment. The control subjects met the following inclusion criteria: free of neurological or musculoskeletal disability, joint pathologies or bone lesions in upper extremities.

To obtain diagnostic data, all spastic patients were clinically evaluated by an experienced clinician using Brunnstrom Recovery Stage and Modified Ashworth Scale. The demographic characteristics of the patients are summarized

Fig. 3. Overview of the experimental setup. For each subject, the initial position of the elbow joint was defined as the maximum flexion allowed by the approximation of the upper-arm and the forearm, and the final position was defined as the maximum extension of the joint. The spasticity phenomenon in the elbow flexors and extensors was evaluated by stretching the handle to make the joint passively move from the initial position towards the final position at an arbitrary velocity.

TABLE II
DEMOGRAPHIC AND CLINICAL CHARACTERISTICS OF PATIENTS

ID	Age (years)	Gender (M/F)	Etiology	Side (L/R)	BRS	MAS
1	36	M	Hemorrhagic	L	II	2
2	53	M	Ischemic	L	IV	0
3	37	M	Ischemic	L	III	1+
4	32	M	Hemorrhagic	R	I	3
5	67	F	Ischemic	L	II	2
6	52	M	Ischemic	R	I	3
7	61	F	Hemorrhagic	R	IV	1
8	48	F	Ischemic	R	IV	1+
9	63	M	Ischemic	L	I	2
10	72	M	Ischemic	L	V	1
11	40	M	Ischemic	R	IV	1+
12	66	F	Hemorrhagic	R	IV	1
13	41	M	Ischemic	L	III	2
14	43	M	Hemorrhagic	L	II	2
15	75	F	Ischemic	R	I	3
16	39	M	Hemorrhagic	R	III	2

* BRS = Brunnstrom Recovery Stage, MAS = Modified Ashworth Scale, M/F = Male or Female, L/R = Left or Right; Clinical examination was carried out for the upper extremity of the more impaired side.

in Table II. The study was reviewed and approved by the Ethics Committee of China Rehabilitation Research Center, and written informed consent was provided by each subject after notified of experimental procedures.

B. Experimental Protocol

In this study, elbow flexor and extensor spasticity was assessed in three sessions by considering the velocity-dependent characteristics of spastic behaviors. To begin with, the subject was seated on an adjustable chair and the developed assessment device was mounted on the upper limb using a self-adhesive belt (i.e. the more affected side for the patient or the non-dominant side for the healthy control). To measure the maximum range of motion for elbow flexion and extension, the subject was instructed to relax completely, and an experienced clinician pushed or pulled the holding handle to slowly move the subject's forearm through the maximum range allowed by the elbow joint. During slow stretches, the joint angles for the subject-specific full flexion and full extension can be recorded.

The following three sessions were designed to evoke the subject's stretch reflex responses at different stretch velocities (i.e. slow (60-99°/s), moderate (100-139°/s) and fast (140-180°/s)), and each session consists of three stretch movements from the full flexion to full extension (see Fig. 3). Specifically, the subject stayed seated with the arm coupled with the assessment device. After a 'go' signal, the forearm was stretched through the handle from maximal flexion towards maximal extension, and then returned to the starting position at the end of a trial. A metronome was used to instruct the clinician to perform slow, moderate and fast trials. As the motor unit is recruited by a minimum time of 6 s during the repeated muscle contractions, different sessions were separated by a rest of 10 s to avoid muscle accommodation effect [27], [28].

C. Data Preprocessing

1) Kinematic Data: The joint angle measured by the angle-position sensor was smoothed using a Kalman filter, which also calculated the angular velocity and angular acceleration to avoid high-frequency noise introduced by numerical derivatives. First, we defined the joint angle, angular velocity and acceleration as state variables and a linear discrete-time model can be built for the elbow joint:

$$\begin{aligned} x_k &= Gx_{k-1} + \omega_{k-1}, \quad \omega \sim N(0, Q) \\ y_k &= Cx_k + \upsilon_k, \quad \upsilon \sim N(0, R), \end{aligned} \tag{1}$$

where $x_k = \left[\theta_k\ \dot{\theta}_k\ \ddot{\theta}_k\right]^T$ refers to the kth estimated state, y_k refers to the kth value of the elbow joint angle, ω and υ are the systematic noise and measurement noise respectively, and

$$G = \begin{bmatrix} 1 & T_s & \frac{1}{2}{T_s}^2 \\ 0 & 1 & T_s \\ 0 & 0 & 1 \end{bmatrix}$$
$$C = [1 \quad 0 \quad 0]$$

Then, the filter algorithm predicted the current state in terms of the minimization of mean square error. The filtered angle, velocity and acceleration could be calculated based on the current measurement of joint angle and the last estimation of three state variables. The iterative process consisting of the

state prediction, covariance prediction, Kalman gain calculation, state update and covariance update can be formulated as follows:

$$\begin{cases} \hat{x}(k|k-1) = G\hat{x}(k-1|k-1) \\ P(k|k-1) = GP(k-1|k-1)G^T + Q \\ K = \dfrac{P(k|k-1)C^T}{CP(k|k-1)C^T + R} \\ \hat{x}(k|k) = \hat{x}(k|k-1) + K(Z(k) - C\hat{x}(k|k-1)) \\ P(k|k) = (I - KC)P(k|k-1), \end{cases} \tag{2}$$

where Q and R denote the covariance of ω and υ, K is the Kalman gain, and P is the covariance matrix of the estimation error.

2) Biomechanical Data: The measured torques were smoothed using a Butterworth low-pass filter (cut-off frequency: 20 Hz) to remove noises.

3) Electrophysiological Data: The raw sEMG signals were first filtered using a Butterworth band-pass filter with low/high cut-off frequencies 20/200 Hz. Then the three-channel sEMG signals were separately rectified to extract the envelope:

$$sEMG^m_{fwr}(k) = \left| sEMG^m_f(k) \right|, \tag{3}$$

where $sEMG^m_f(k)$ denotes the kth filtered sEMG signal in the mth channel, and $sEMG^m_{fwr}(k)$ denotes the corresponding sEMG signal after full-wave rectification. In the following, a Butterworth low-pass filter (cut-off frequency: 5 Hz) was used to remove the noise introduced by the above rectification.

IV. Multi-Layer Architecture for Spasticity Assessment

A. Mechanical Impedance Identification

Mechanical impedance of human joints characterizes the dynamic relationship between force and kinematics under external perturbation, and serves as a good basis for analyzing the changes in joint properties resulting from abnormal muscle tone. Therefore, we parameterized the instantaneous dynamic impedance of human elbow joint by a second-order model, i.e., the time-varying stiffness, damping and inertia function:

$$\tau(t) = I(t)\ddot{\theta} + B(t|\theta, \dot{\theta}, \mu)\dot{\theta} + K(t|\theta, \dot{\theta}, \mu)(\theta - \theta_0), \tag{4}$$

where $\tau(t)$ is the torque responses to the impose limb stretches, θ, $\dot{\theta}$ and $\ddot{\theta}$ are the joint angle, angular velocity and acceleration derived from the Kalman filter, respectively, θ_0 is the equilibrium position of elbow joint, μ is the muscle activation vector, I is the total inertia component of the upper limb and other coupled body segments, B and K are the joint damping and stiffness components, respectively.

As the joint torque was mainly determined by torque perturbation applied by the clinician, we can rewrite the model as:

$$\tau_p(t) = I(t)\ddot{\theta} + B(t|\theta, \dot{\theta}, \mu)\dot{\theta} + K(t|\theta, \dot{\theta}, \mu)(\theta - \theta_0) + GL\cos(\theta) \tag{5}$$

where the external perturbation $\tau_p(t)$ was recorded at each time point, G and L are the gravity of the forearm and the moment arm, which were estimated on the basis of the height and weight, according to anthropometric database of adult population.

Among different identification approaches such as the least-squares method [29], neural network method [30] and evolutionary computation technique [31], we used a GA-based identification method to identify the dynamic impedance parameters in the time-varying system, due to the capability of GA to search for global optimum without assumptions about the search space.

Considering the balance between the identification accuracy and the computational burden, one set of unknown parameters were identified from the full flexion to full extension for each stretch trial. The proposed identification method consisted of six steps:

Step 1: Initialize the chromosome population by real-value encoding. Since the equilibrium position cannot be accurately determined in each motion segment, I, B, K, as well as the combination of K and θ_0 are evolutionally identified within a population of T chromosomes.

Step 2: Calculate the fitness value of each individual, and select a group of individuals most successful in this "competition".

Step 3: Apply crossover operator to the "surviving" population under the probabilistic probability P_c, and produce new offsprings. Calculate the fitness values for all individuals, and preserve a new population of T chromosomes.

Step 4: Apply mutation operator to the new population under the probabilistic probability P_m, and produce new offsprings. Calculate the fitness values for all individuals, and preserve a new population of T chromosomes.

Step 5: Go to Step 2.

Step 6: If the fitness value satisfies the stopping criterion or the generation number is enough, the algorithm ends. If not, go to Step 3.

In this study, we defined the initial population size $T = 50$ to ensure the speed of convergence but without increasing computational expensive. The combination of I, B, K and $K\theta_0$ was optimized by the proposed algorithm, which makes the fitness function minimum:

$$\varepsilon = \sqrt{\frac{1}{M}\sum_{t=1}^{M}(\tau_p(t) - \tau_{est}(t))^2}, \tag{6}$$

where M is the sample size of the current motion segment, $\tau_p(t)$ and $\tau_{est}(t)$ are the measured and estimated torques, respectively.

Furthermore, the crossover and mutation probabilities were proportional to the fitness value, therefore, genes from the better individuals can propagate into the next generation as much as possible. We also applied an elite strategy to transfer the better solution into the next generation without any changes.

B. Neurophysiological Feature Extraction

As the spastic behavior is caused by the lesion in the descending inhibition of supraspinal motor pathways, the manifestation of spastic muscles includes the involuntary and unconscious changes in the electrophysiological output. In order to quantify the electrophysiological responses evoked

by different stretch velocities, we started by applying EEMD to decompose the non-stationary sEMG signals into a series of intrinsic mode functions (IMFs), thereby extracting time-domain features from these multi-resolution components.

To begin with, the white Gaussian noise was added to reconstruct the biceps brachii sEMG signals with uniform distribution:

$$x_i(t) = x(t) + w_i(t) \tag{7}$$

where $x(t)$ is the preprocessing sEMG signals, and $w_i(t)$ is the identically distributed white noise. The iterative procedures to decompose the noisy signal $x_i(t)$ into IMFs consisted of the following steps:

Step 1: Identify all the local maxima and minima for the given time series, and interpolate through the local maxima and minima respectively, to create the upper envelope $e_i^+(t)$ and lower envelope $e_i^-(t)$, respectively.

Step 2: Calculate the mean of the two envelopes, and subtract it from the data signal, resulting in the first component:

$$\begin{aligned} m_i^h(t) &= \frac{(e_i^+(t) \ + e_i^-(t))}{2} \\ h_i^h(t) &= x_i(t) - m_i^h(t) \end{aligned} \tag{8}$$

Step 3: Repeat the sifting process (i.e. Step 1 and Step 2) for the new data signal $x_i(t) = h_i^h(t)$ until coincides with the properties of IMFs:

- the number of zero crossings and the number of local maxima must be equal or differ at most by one;
- the mean value of the upper and lower envelopes must be equal to zero.

Step 4: Separate the IMF $c_i^h(t) = h_i^h(t)$ from the given data, and apply the aforementioned steps repetitively on the residual signal:

$$r_i^1(t) = x_i(t) - c_i^1(t), \ldots, r_i^n(t) = r_i^{n-1}(t) - c_i^n(t) \tag{9}$$

Step 5: The decomposition process continues to find the IMF containing lower frequency oscillations until the residual signal $r_i^n(t)$ becomes a monotonic function or has only one extremum.

After multi-level decomposition, the input sEMG signal can be reconstructed:

$$x_i(t) = \sum_{h=1}^{n} c_i^h(t) + r_i^n(t) \tag{10}$$

where $r_i^n(t)$ refers to the final residual after the extraction of nth IMFs components.

We added identically distributed white noise to the original signal multiple times, and the above procedures were repeated to extract the corresponding IMFs. Furthermore, the optimum choice of each decomposition level can be determined by:

$$IMF^h = \frac{1}{N} \sum_{i=1}^{N} c_i^h(t) \tag{11}$$

where $N = 50$ is the number of noise adding, and IMF^h is the hth ensemble IMF components. It is worth mentioning that the standard deviation of noise was set to 0.2 times the standard deviation of the sEMG signals.

Given the first three IMFs carried most of the valuable information of the sEMG signals, the mean absolute variation (MAV) and root mean square (RMS) were extracted from the corresponding IMFs, which can reveal how the magnitudes of each IMF change due to the hyperexcitability of stretch reflexes, and were calculated as follows:

$$\begin{aligned} \nu_k &= \frac{1}{M-1} \sum_{t=2}^{M} \left| IMF^h(t) - IMF^h(t-1) \right| \\ \sigma_k &= \sqrt{\frac{1}{M} \sum_{t=1}^{M} \left(IMF^h(t) \right)^2}, \end{aligned} \tag{12}$$

where M have been defined above.

Since there are evidences that the impairments in spastic patients is mainly due to three disturbances including decreased muscle activation, decreased threshold of stretch reflexes and stereotypical muscle co-activation, we further estimated the TSRT value of biceps brachii sEMG signals by extrapolating the linear regression line through DSRT values of various stretch velocities to yield intercept with the joint angle axis, specifically, the DSRT value was identified as the joint angle when the sEMG signal increased by two times of standard deviations above the mean baseline signal.

To quantify the pathological phenomenon in agonist recruitment and antagonist inhibition, the co-activation features among pronator teres, biceps brachii and triceps brachii were extracted by calculating the co-activation ratio:

$$\begin{aligned} CR_1 &= \frac{\int_{t_1}^{t_2} \left| sEMG^1(t) \right| dt}{\int_{t_1}^{t_2} \left| sEMG^1(t) \right| dt + \int_{t_1}^{t_2} \left| sEMG^3(t) \right| dt} \\ CR_2 &= \frac{\int_{t_1}^{t_2} \left| sEMG^2(t) \right| dt}{\int_{t_1}^{t_2} \left| sEMG^2(t) \right| dt + \int_{t_1}^{t_2} \left| sEMG^3(t) \right| dt} \end{aligned} \tag{13}$$

where $sEMG^1(t)$, $sEMG^2(t)$ and $sEMG^3(t)$ refer to the preprocessing sEMG signals of pronator teres, biceps brachii and triceps brachii respectively, t_1 and t_2 are the starting and ending times of a stretch trial.

C. Multi-Level Fusion Scheme

In this section, we developed an multi-level regression model to automatically fuse the quantification of kinematic, biomechanical and electrophysiological impairments, since spastic behaviors have been attributed to the alterations of mechanical and neuronal properties, further combination of multi-level features can facilitate a more comprehensive assessment result (see Fig. 4).

To begin with, we defined an experimental sample as the multi-modal information acquired in a stretch trial, as the mechanical impedance of elbow joint was identified and the activation features of related muscles were extracted, the input vector of the regression model was constituted:

$$Q_i = \left[\mu_1, \ldots, \mu_n, \ldots, \mu_{N_F} \right]^T, \tag{14}$$

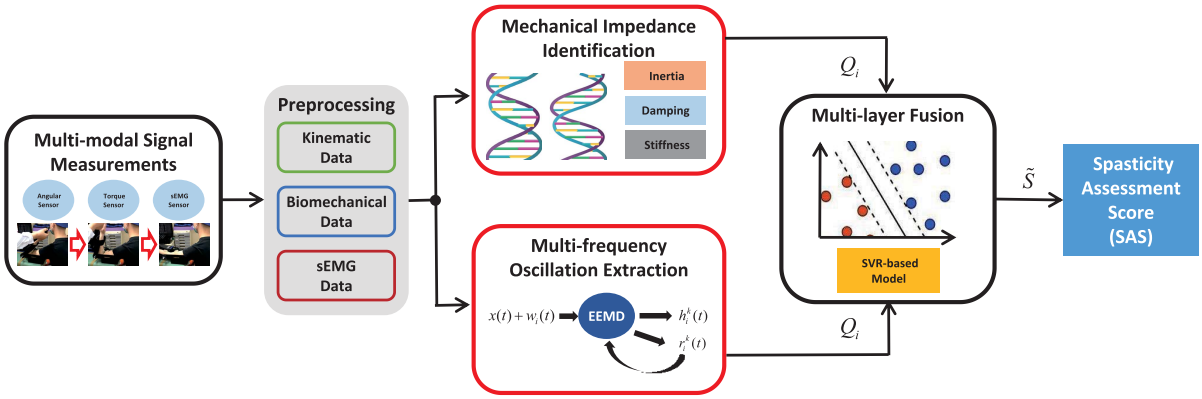

Fig. 4. The multi-layer architecture for assessing the severity level of the upper-limb spasticity. The multi-modal signals collected in the passive stretches served as the input vector of the proposed assessment architecture. The mechanical impedance components of the human elbow joint was identified using the GA-based method to quantify the spastic resistance judged in clinical practices, while the sparsely distributed sEMG signals were decomposed using the EEMD method to reveal the neurophysiological abnormalities resulting in spastic behaviors. These single-layer decisions Q_i were further fused by a SVR-based model to create an overall quantification of the spasticity severity $\tilde{S}$.

where μ_n denotes the induced stretch velocity, major impedance parameters (i.e. damping and stiffness components), as well as the MAV, RMS and CR values of spastic muscles, $N_F = 11$ stands for the dimension of the feature vector. Note that the corresponding ground truth was set to the MAS score given by the clinician. Because the inconvenient category of 1+ in the MAS results, the 1+ score was re-assigned to a value of 1.5. By adopting the supervised machine learning approach, the prediction for severity estimation of spasticity can be obtained:

$$S_i = F(Q_i), \tag{15}$$

where F denotes the fusion model constructed by the support vector regression (SVR), in which the kernel was selected as the radial basis function.

Furthermore, the severity predictions belonging to per participant were fused as follows:

$$\tilde{S} = \frac{1}{J}\sum_{i=1}^{J} S_i, \tag{16}$$

where $\tilde{S}$ stands for the spasticity assessment score (SAS) that reliably quantify the spastic hypertonia. It can be derived that a lower SAS score indicates that the upper-limb motor function approaches a better status.

To improve the generalization performance of the multi-layer assessment architecture, the full dataset consisting of multi-modal data measured in 234 trials was separated into two non-overlapping parts: the training dataset comprised 144 experimental samples collected from 16 individuals (i.e. 9 samples can be extracted from 9 evoked stretch trials for each individual), and the remaining samples were divided into the test dataset. Concretely, the hyper-parameters of the fusion model were optimized by 5-fold cross validation procedures.

V. Results

A. Identification Performance

Given the crucial role of mechanical impedance identification in the quantitative assessment of spasticity phenomenon,

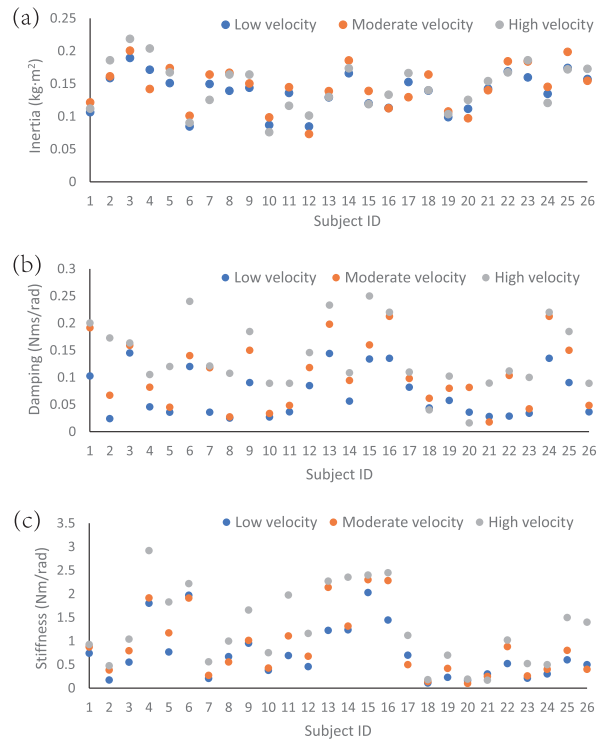

Fig. 5. Quantitative identification results for: (a) inertia, (b) damping and (c) stiffness components of the elbow joint. The blue, orange and gray circles represent the impedance parameters averaged over stretch trials with low, moderate and high velocities, respectively.

we started by investigating the identification reliability of the inertia, damping and stiffness parameters, thereby analyzing the biomechanical variation evoked by external perturbation. Fig. 5 illustrates the identification results of the second-order impedance model using the GA-based approach for all spastic and control subjects.

The values of inertia component were found to be more clustered than that of the damping and stiffness components across subjects, which can be attributed to the fact that the human upper extremity has a certain inertia, most of the

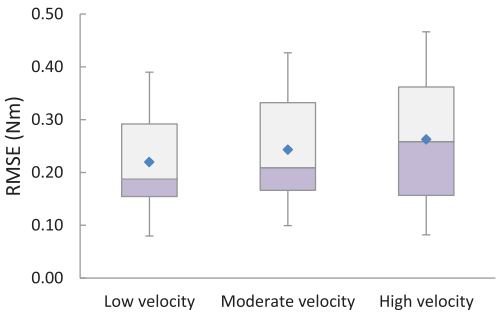

Fig. 6. Identification performance distributions under different velocity patterns. The blue dot and black line refer to the mean and median of the corresponding RMSE, respectively.

time assumed to be dependent on the structural parameters. The damping and stiffness components showed a clear trend of clustering under different stretch velocities for spastic patients, and the identification values became higher when the velocity of the imposed stretches increased. These results were consistent with the velocity-dependent characteristics of spasticity emphasized in previous studies, and demonstrated that the proposed architecture has the potential to distinguish between spastic hypertonia versus normal muscle tone.

Furthermore, we reported the identification performance in terms of the root mean square error (RMSE):

$$\varepsilon_i = \sqrt{\frac{\sum_{t=1}^{M}\left[\tau(t) - \tilde{I}\ddot{\theta} - \tilde{B}\dot{\theta} - \tilde{K}\theta - N(t)\right]^2}{M}} \tag{17}$$

where ε_i denotes the overall estimation error for the ith trial, M is the sample size from maximal flexion towards maximal extension in the current trial, $\tilde{I}$, $\tilde{B}$ and $\tilde{K}$ refers to the GA-based estimations of the inertia, damping and stiffness parameters belonging to this motion segment, $N(t)$ represents the bias term including the joint torque at the equilibrium position and the gravity of the subject's forearm.

The estimation error distributions of low, moderate and high stretch velocities are visualized in Fig. 6. Averaging across subjects, the mean RMSE between the estimated resistance torque and the measurements was 0.22 Nm with a standard deviation 0.09 Nm for the slow stretch movements, as well as 0.24 ± 0.10 Nm and 0.26 ± 0.12 Nm for the moderate and high velocity patterns. It can be seen that the dynamic impedance model was accurately identified by integrating the elite preservation policy into the evolutionary computation algorithm. These promising results revealed how the viscoelastic properties of the spastic arm change underlying the mechanical resistance manually rated by clinical scales, and further serve as a good basis for the reliable assessment of motor deficits in spastic patients.

B. Quantification Performance

Since our purpose is to enable quantitative and comprehensive assessment of spasticity symptoms, it is essential to investigate whether the multi-layer architecture can yield an easy-to-understand index significantly correlated with clinical scores for the spasticity severity quantification.

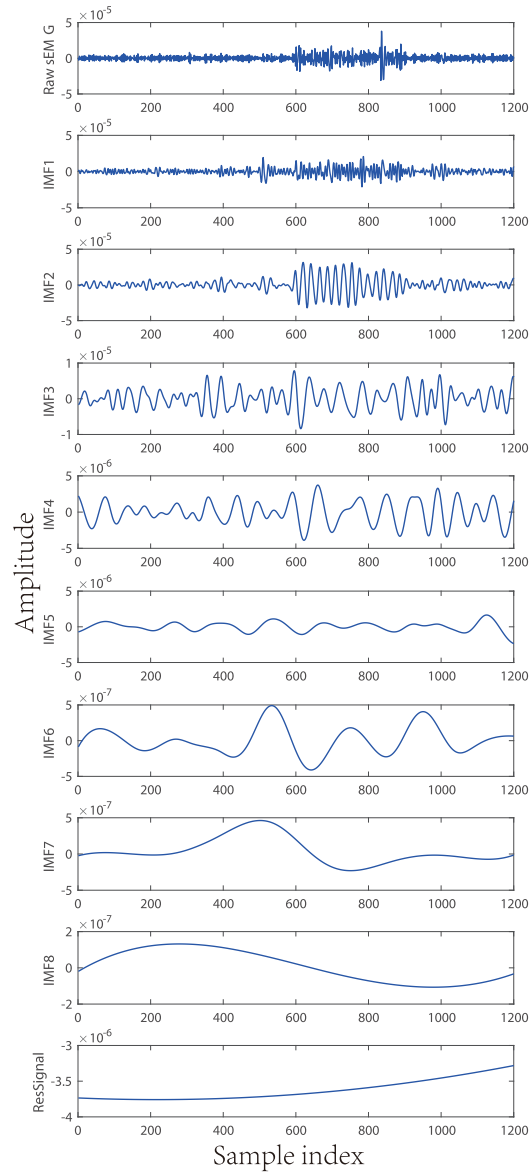

Fig. 7. Representative results of sEMG signal decomposition.

To account for the alterations in neural component of spastic behaviors, we employed EEMD to decompose the sEMG signal into multi-dimensional signals, which can reflect morphological changes in the non-linear and non-stationary signals more precisely. Fig. 7 presents the adaptive decomposition results containing a set of IMF components for a representative stretch trial. We can observe that the frequency oscillations in each IMF were lower than that in the preceding one. By selecting appropriate IMFs, the statistical features were extracted to serve as an input vector for the fusion model.

Subsequently, the identified dynamic impedance and the above electrophysiological features were concatenated together, and fed into the supervised fusion model. In order to validate the quantification performance of multi-layer architecture, we calculated the RMSE between the SASs and the MAS scores based on the independent training dataset and test dataset. Averaging across trials, the RMSE values are 0.25 and 0.39 for the training dataset and test dataset

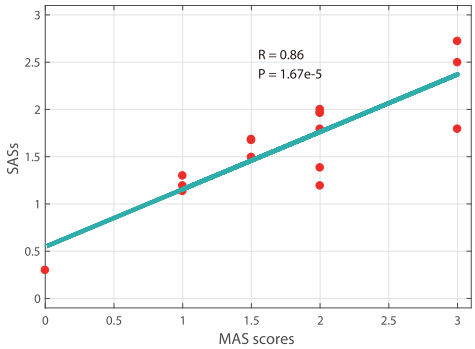

Fig. 8. Correlation analysis between the SASs and the MAS scores.

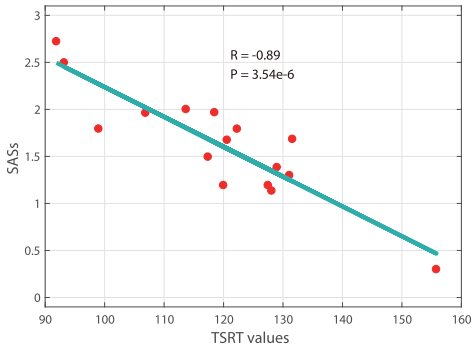

Fig. 9. Correlation analysis between the SASs and the TSRT values.

respectively, which indicates that the propose index was consistent with the clinical scale, and capable of reliably quantifying the severity level of the spasticity.

Furthermore, we performed Pearson correlation test [32] with 95% confidence intervals to analyze the correlation between the SASs and the MAS scores. The results of correlation analysis and the corresponding Pearson correlation coefficients are shown in Fig. 8. As can be seen, the proposed index exhibited a positive relationship with the MAS score ($R = 0.86$, $P < 0.0001$). Therefore, by exploring the complementarity of kinematic, biomechanical and electrophysiological characteristics, the developed system can yield a quantitative score with superior clinical relevance.

As numerous previous studies have found that the TSRT is an emerging measurement widely used to quantify the severity of the spasticity by considering the velocity-dependent onset of stretch reflex activities, the correlation analysis was also carried out to demonstrate the association between the SASs and the TSRT values. Fig. 9 depicts the correlation analysis results for all spastic subjects. We found a negative correlation between the SASs and the TSRT derived from biceps brachii sEMG signals ($R = -0.89$, $P < 0.0001$), which was well agreed with the previous observation, i.e., the lower the TSRT value, the severer the spasticity progression.

In more detail, the assessment system not only provided a more comprehensive quantification of upper-limb spasticity, but also achieved more precise discrimination of the level of spasticity. For example, the subjects with ID of 1 and 5 have the same MAS grades (i.e. more marked increase in muscle tone), which means the amount of resistance to imposed stretches is hard to be distinguished manually. The SASs obtained from the proposed system, however, are 1.19 and 1.96 for subject 1 and subject 5, indicating that the spasticity symptoms in subject 5 are severer than that in subject 1, and the corresponding TSRT values of 127.50 and 106.90 also prove the difference in spasticity severity. Therefore, the proposed index improves the sensitivity of the upper-limb spasticity assessment, and features extracted from different layers are capable of offering detailed information for the personalized treatment design.

VI. Discussion and Conclusion

The purpose of this study is to develop an assessment system to comprehensively quantify the upper-limb spasticity of post-stroke patients. By designing an exoskeletal assessment device, multi-modal data was synchronously recorded during passive stretch motion under a range of velocities. As the mechanical impedance can delineate the biomechanical responses underlying the spastic resistance manually graded in conventional clinical scales, we started by identifying a parametric impedance model consisting of inertia, damping and stiffness using the modified genetic algorithm. To quantify the abnormalities in neurophysiological level, the biceps brachii sEMG signals were decomposed into a series of IMFs through EEMD process, from which the electrophysiological features were extracted. By concatenating the quantification output of biomechanical and neurophysiological levels, a fusion model was constructed based on the SVR to generate a more reliable spasticity severity score. Experimental results demonstrated that the proposed system exhibited superior performance in quantifying the spasticity symptoms with significant clinical relevance.

To our knowledge, the identification of mechanical impedance has seldom been integrated into upper-limb spasticity assessment systems, and ours is the first study to simultaneously quantify the changes of mechanical and neuronal properties of the spastic limb. By using the elite preservation policy, the GA exhibited superior performance in the impedance parameter estimation, as shown in Fig. 6. Specifically, the quantification of abnormal joint stiffness and damping has been proven to have inter-subject reliability in distinguishing spastic patients from healthy controls, which is suitable to serve as an objective indicator of spastic hypertonia.

As the sEMG signals of spastic muscles are non-stationary and seem chaotic during the induced stretch reflex, we adopted EEMD to process the sparsely distributed sEMG signals, and then extracted the time-frequency features to provide in-depth information about the agonist recruitment and antagonist inhibition underlying spastic behaviors. Compared with the TSRT measurement algorithm focusing only on the time-domain parameters, the proposed electrophysiological analysis put the emphasis on the time-varying frequency distributions of the muscle activation and co-activation.

Unlike the previous studies that have been so far limited to evaluate the behavioral abnormalities of spasticity in

a specific level, our assessment system used a SVR-based fusion scheme to further exploit the complementarity among kinematic, biomechanical and electrophysiological characteristics. In general, the proposed system provides an easy-to-use tool that enables reliable monitoring of spasticity progression, as well as the objective efficacy evaluation of the existing treatment. Furthermore, future research with larger sample size will be pursued to better improve the generalizability of the multi-layer architecture.

References

[1] J. W. Lance, "The control of muscle tone, reflexes, and movement: Robert Wartenbeg lecture," *Neurology*, vol. 30, no. 12, p. 1303, 1980.

[2] G. Sheean, "The pathophysiology of spasticity," *Eur. J. Neurol.*, vol. 9, pp. 3–9, May 2002.

[3] A. Pandyan *et al.*, "Spasticity: Clinical perceptions, neurological realities and meaningful measurement," *Disability Rehabil.*, vol. 27, nos. 1–2, pp. 2–6, Jan. 2005.

[4] A. W. Dromerick, "Clinical features of spasticity and principles of treatment," in *Clinical Evaluation and Management of Spasticity*. Totowa, NJ, USA: Humana Press, 2002, pp. 13–26.

[5] J. W. Lance, "Pathophysiology of spasticity and clinical experience with baclofen," in *Spasticity: Disordered Motor Control*, J. W. Lance, R. G. Feldman, R. R. Young, and W. P. Koella, Eds. Chicago, IL, USA: Year Book, 1980, pp. 185–204.

[6] R. T. Katz and W. Z. Rymer, "Spastic hypertonia: Mechanisms and measurement," *Archi. Phys. Med. Rehabil.*, vol. 70, no. 2, pp. 144–155, 1989.

[7] L. R. Logan, "Rehabilitation techniques to maximize spasticity management," *Topics Stroke Rehabil.*, vol. 18, no. 3, pp. 203–211, May 2011.

[8] G. Sheean and J. R. McGuire, "Spastic hypertonia and movement disorders: Pathophysiology, clinical presentation, and quantification," *PM&R*, vol. 1, no. 9, pp. 827–833, Sep. 2009.

[9] F. Biering-Sørensen, J. B. Nielsen, and K. Klinge, "Spasticity-assessment: A review," *Spinal Cord*, vol. 44, no. 12, pp. 708–722, Dec. 2006.

[10] B. Ashworth, "Preliminary trial of carisoprodal in multiple sclerosis," *Practitioner*, vol. 192, pp. 540–542, 1964.

[11] R. Bohannon and M. Smith, "Upper extremity strength deficits in hemiplegic stroke patients: Relationship between admission and discharge assessment and time since onset," *Arch. Phys. Med. Rehabil.*, vol. 68, no. 3, pp. 155–157, 1987.

[12] G. Tardieu, "A la recherche d'une technique de mesure de la spasticite," *Revue Neurologique*, vol. 91, no. 2, pp. 143–144, 1954.

[13] J. Mehrholz *et al.*, "Reliability of the modified tardieu scale and the modified Ashworth scale in adult patients with severe brain injury: A comparison study," *Clin. Rehabil.*, vol. 19, no. 7, pp. 751–759, Nov. 2005.

[14] J. Mehrholz, Y. Major, D. Meißner, S. Sandi-Gahun, R. Koch, and M. Pohl, "The influence of contractures and variation in measurement stretching velocity on the reliability of the modified Ashworth scale in patients with severe brain injury," *Clin. Rehabil.*, vol. 19, no. 1, pp. 63–72, Feb. 2005.

[15] A. D. Pandyan, G. R. Johnson, C. I. M. Price, R. H. Curless, M. P. Barnes, and H. Rodgers, "A review of the properties and limitations of the Ashworth and modified Ashworth scales as measures of spasticity," *Clin. Rehabil.*, vol. 13, no. 5, pp. 373–383, Oct. 1999.

[16] W. K. L. Yam and M. S. M. Leung, "Interrater reliability of modified Ashworth scale and modified Tardieu scale in children with spastic cerebral palsy," *J. Child Neurol.*, vol. 21, no. 12, pp. 1031–1035, Dec. 2006.

[17] A. Calota, A. G. Feldman, and M. F. Levin, "Spasticity measurement based on tonic stretch reflex threshold in stroke using a portable device," *Clin. Neurophysiol.*, vol. 119, no. 10, pp. 2329–2337, Oct. 2008.

[18] K. S. Kim, J. H. Seo, and C. G. Song, "Portable measurement system for the objective evaluation of the spasticity of hemiplegic patients based on the tonic stretch reflex threshold," *Med. Eng. Phys.*, vol. 33, no. 1, pp. 62–69, Jan. 2011.

[19] C. A. McGibbon, A. Sexton, M. Jones, and C. O'Connell, "Elbow spasticity during passive stretch-reflex: Clinical evaluation using a wearable sensor system," *J. Neuroeng. Rehabil.*, vol. 10, no. 1, pp. 1–14, 2013.

[20] B. Hu *et al.*, "Spasticity measurement based on the HHT marginal spectrum entropy of sEMG using a portable system: A preliminary study," *IEEE Trans. Neural Syst. Rehabil. Eng.*, vol. 26, no. 7, pp. 1424–1434, Jul. 2018.

[21] Y.-S. Yang, Z. F. Emzain, and S.-C. Huang, "Biomechanical evaluation of dynamic splint based on pulley rotation design for management of hand spasticity," *IEEE Trans. Neural Syst. Rehabil. Eng.*, vol. 29, pp. 683–689, 2021.

[22] W. S. Ang, H. Geyer, I.-M. Chen, and W. T. Ang, "Objective assessment of spasticity with a method based on a human upper limb model," *IEEE Trans. Neural Syst. Rehabil. Eng.*, vol. 26, no. 7, pp. 1414–1423, Jul. 2018.

[23] H. Wang *et al.*, "Assessment of elbow spasticity with surface electromyography and mechanomyography based on support vector machine," in *Proc. 39th Annu. Int. Conf. IEEE Eng. Med. Biol. Soc. (EMBC)*, Jul. 2017, pp. 3860–3863.

[24] M. F. Levin and A. G. Feldman, "The role of stretch reflex threshold regulation in normal and impaired motor control," *Brain Res.*, vol. 657, nos. 1–2, pp. 23–30, Sep. 1994.

[25] C. P. Phadke, F. Ismail, and C. Boulias, "Current challenges to clinical assessment of spasticity," *Int. J. Neurol. Res.*, vol. 1, no. 1, pp. 1–4, 2015.

[26] N. K. Musampa, P. A. Mathieu, and M. F. Levin, "Relationship between stretch reflex thresholds and voluntary arm muscle activation in patients with spasticity," *Exp. Brain Res.*, vol. 181, no. 4, pp. 579–593, Jul. 2007.

[27] M. Gorassini, J. F. Yang, M. Siu, and D. J. Bennett, "Intrinsic activation of human motoneurons: Reduction of motor unit recruitment thresholds by repeated contractions," *J. Neurophysiol.*, vol. 87, no. 4, pp. 1859–1866, Apr. 2002.

[28] G. E. Nuyens, W. J. De Weerdt, A. J. Spaepen, C. Kiekens, and H. M. Feys, "Reduction of spastic hypertonia during repeated passive knee movements in stroke patients," *Arch. Phys. Med. Rehabil.*, vol. 83, no. 7, pp. 930–935, Jul. 2002.

[29] A. L. Shorter and E. J. Rouse, "Ankle mechanical impedance during the stance phase of running," *IEEE Trans. Biomed. Eng.*, vol. 67, no. 6, pp. 1595–1603, Jun. 2020.

[30] U. Demir, S. Kocaoğlu, and E. Akdoğan, "Human impedance parameter estimation using artificial neural network for modelling physiotherapist motion," *Biocybern. Biomed. Eng.*, vol. 36, no. 2, pp. 318–326, 2016.

[31] J. Wua, J. Wanga, and Z. You, "An overview of dynamic parameter identification of robots," *Robot. Comput. Integr. Manuf.*, vol. 26, no. 5, pp. 414–419, 2010.

[32] J. Benesty, J. Chen, Y. Huang, and I. Cohen, "Pearson correlation coefficient," in *Noise Reduction in Speech Processing*. Berlin, Germany: Springer, 2009, pp. 1–4.